JOURNAL OF PROPULSION AND POWER
Vol. 15, No. 1, January–February 1999

Single-Point Thermometry in High-Pressure, Sooting, Premixed Combustion Environments

Michael S. Brown*
MetroLaser, Inc., Irvine, California 92614
and
William L. Roberts†
North Carolina State University, Raleigh, North Carolina 27695

We have performed nonintrusive thermometry in the burnt gases of rich, pressurized ethylene/air flames using a frequency measurement based on laser-induced gratings. Light from a continuous-wave probe beam is coherently scattered from a thermal or electrostrictive grating induced by a pair of crossed, pulsed pump beams. The measured Doppler shift of the signal beam is a function of the local speed of sound from which a temperature can be extracted. At equivalence ratios of 1.6, the transient grating temperature agreed with a corrected thermocouple temperature. At higher soot loading, it is necessary to account for the change in local gas composition caused by soot particle vaporization. Soot particles, acting as blackbody absorbers, were observed to generate thermal gratings of diagnostic value.

Nomenclature

A_{rad} = radiative decay rate, s^{-1}
$a(\tau_{las})$ = soot particle radius after laser heating, nm
a_0 = initial soot particle radius, nm
B = second virial coefficient, cm^3/mol
C_p = heat capacity at constant pressure, J/K mole
C_T = gas compressibility, dyne/cm^2
c = speed of light, cm/s
D_s = mass diffusivity, cm^2/s
D_t = thermal diffusivity, cm^2/s
f_B = transient grating spectroscopy signal frequency, Hz
f_v = soot volume fraction, ppm
$G(\theta, r_{pr}, r_p)$ = geometric weighting factor
$g_{las}(t)$ = Gaussian pulse shape of pump laser beams
I = pump beam intensity, W/cm^2
L = length of laser-induced grating, cm
M = gram molecular mass of gas mixture, g/mole
M_{vap} = numer of soot fragment moles expelled from one vaporizing soot particle
m_{C_n} = gram molecular weight of soot fragments C_n, g/mole
N_A = Avogadro's number
N_{C_n} = number density of soot particle fragments, cm^{-3}
N_{gases} = number density of combustion gases, cm^{-3}
N_{part} = number density of soot particles, cm^{-3}
n = index of refraction
Q = electronic quenching rate, s^{-1}
q = grating wave vector, $2\pi/\Lambda$, cm^{-1}
R = universal gas constant
r_p = radius of pump beams, μm
r_{pr} = radius of probe beam, μm
T = temperature, K
V_m = molar volume, cm^3/mole
x_{C_n} = mole fraction of C_n soot fragments
α = absorption coefficient, cm^{-1}
β = correction factor for finite beam width, s^{-1}
Γ = acoustic damping coefficient, $0.5[(\gamma - 1) + 4\gamma/(9\gamma - 5)]D_t$, cm^2/s
Γ_e = electrostrictive coefficient, $(n^2 - 1)(n^2 + 2)/3$
γ = specific heat ratio
Δn = perturbation of index of refraction
η = light scattering efficiency
θ = angular separation of pump beams, rad
Λ = grating fringe spacing, μm
λ = pump beam wavelength, nm
λ_{pr} = probe beam wavelength, nm
ρ = gas density, mole/cm^3
τ_p = pump laser pulse width, ns
ϕ = fraction of absorbed energy collisionally transferred to surrounding gas
ψ = arbitrary scaling factor
ω_B = Brillouin frequency, $2\pi f_B$, rad/s

Presented as Paper 97-3038 at the AIAA/ASME/SAE/ASEE 33rd Joint Propulsion Conference, Seattle, WA, July 6–9, 1997; received Sept. 30, 1997; revision received June 30, 1998; accepted for publication July 27, 1998.

*Senior Scientist, Applied Spectroscopy Group, 18010 Skypark Circle, Suite 100.

†Assistant Professor, Department of Mechanical and Aerospace Engineering, P.O. Box 7910.

I. Introduction

THE temperature field of combustion environments is a key diagnostic parameter. It reflects the complex interaction of the local chemistry, fluid dynamics, and heat transfer of the combustion gases. For the purposes of testing and validating combustor design and the verification of predictive computer models of combustors, it is imperative that accurate temperature measurements be made in test hardware. Major challenges to optical diagnostics of practical combustors include high pressure, the presence of particulates (particularly soot), a high background luminosity, optical thickness, and limited optical access. These challenges are particularly troublesome for techniques that rely on the accurate measurement of a signal amplitude. To address these issues, we explored a frequency-based technique, transient grating spectroscopy (TGS), for the measurement of temperature in high-pressure, sooting flames. The technique relies on the measurement of the modulation frequency of a laser-induced transient grating signal. This diagnostic is spatially coherent, does not require a tunable laser system, provides spatially resolved information, and has been demonstrated to work at high pressure.[1] The modulation frequency of the signal is sensitive to the local temperature. In the work reported here, we temporally resolved the transient

grating signal generated in a high-pressure, sooting, premixed flame to extract the local temperature.

While it is recognized that time-averaged temperature measurements in a laminar premixed flame are of limited utility to the engine designer, this environment was chosen as a first demonstration of the merits of the TGS technique. In the theory section that follows, the generation of the transient signal is described, as well as the method used to extract the local gas temperature. As explained later in this paper, determination of the local temperature requires some knowledge of the local average molecular mass, M, and the ratio of specific heats, γ. In the postcombustion region of a premixed flame, the major species and, hence, M and γ, are well predicted using a standard chemical equilibrium code. If the fuel is premixed with air, the average molecular weight and ratio of specific heats is fairly insensitive to spatial location because the dominate species is molecular nitrogen. In a diffusion flame, however, there can be significant changes in both M and γ, depending on spatial location relative to the reaction zone. This requires that reasonable values of M and γ be measured in addition to the speed of sound to determine the local gas temperature. Fortunately, there is additional information in the transient grating signal that has not been exploited in this work, but is currently under investigation. The decay of the signal is because of the washing out of the laser-induced grating, caused by diffusion of mass and energy. From the rate of decay of grating reflectivity, diffusion coefficients can be extracted, and from these coefficients, reasonable assumptions can be made about the major gas species present and, hence, M and γ. Thus, while the results presented in this paper are for a premixed sooting flame, the technique has applicability in diffusion-controlled flames as well.

The other simplification in the combustion environment used for this demonstration is that it is laminar and one dimensional, permitting signal averaging, both spatial and temporal. Inherently, however, this technique is an instantaneous, single-shot technique, with measurement times on the order of less than a couple of hundred nanoseconds. This time scale is shorter than even the smallest time scales in subsonic turbulent flows associated with gas turbines. The TGS probe volume will always be an elliptical spheroid, with the dimensions being a function of beam diameter and focal length of the focusing lens. In the results presented in this paper, the long dimension of the probe volume is in the direction of very small gradients, introducing an insignificant error. In a homogeneously turbulent environment, there will always be more spatial averaging in one dimension; this is unavoidable. For this work, the long dimension of the probe volume was about 5 mm, but could be reduced by an order of magnitude if required by the flowfield.

To make nonintrusive temperature measurements in high-pressure, limited optical access combustion environments, the combustion researcher or engine designer has a very limited number of tools available. One technique that has had success in these environments is coherent anti-Stokes Raman spectroscopy.[2] Although CARS is a fairly mature technique, it is still a demanding measurement to make, requiring a tunable laser source, the means to spectrally resolve the signal, and information about the major species present because it is a resonant technique. Quantitative signal analysis requires sophisticated spectral-matching algorithms[3,4] that must include quantum interference affects. In contrast, TGS is nonresonant and, thus, does not require a tunable source or spectral resolution of the signal. The authors believe that the TGS technique, which is not much more difficult to employ than laser Doppler velocimetry (LDV), once it is validated and matured, will be an off-the-shelf technique for thermometry, just as LDV is for velocity measurements.

In short, time-resolved transient grating measurements involve the first-order Bragg scattering of a probe laser off of a grating induced by two crossed pump laser beams. The amplitude and temporal evolution of the spatially coherent signal beam reflects the physical and chemical dynamics of the target medium. The temporal behavior of the signal is a function of the local temperature and transport properties.

Historically, laser-induced grating techniques have been used to explore many time-dependent phenomena in liquids and solids.[5,6] Processes as diverse as the transport of excitons in molecular crystals,[7] the detection of phonons in glassy solids,[8] relaxation modes in liquids,[9] and the kinetics of photoinitiated chemistry in liquids[6] have been studied using this method of forced light scattering. More recently, investigators have applied the technique to gas-phase studies. Experimental work has been performed in static gases at high pressure,[1,10] in the infrared,[11] and in atmospheric flames,[12] and several groups have modeled[13-19] the transient grating signal. While laser-induced grating work is often performed in the time domain, significant frequency domain work has also been reported.[20] Given the quite general applicability of the technique, we chose to study its relevance to combustion research that impacts propulsion engineering.

Transient grating signals are typically generated through one of two physical processes, electrostriction and thermalization. Electrostriction is the acceleration of polarized molecules in a strong electric field gradient. This field-induced movement of the molecules modulates the local density, thereby modulating the local index of refraction. Thermalization is achieved using pump lasers tuned to a molecular resonance of a species present in the test medium. The absorbing species gains electronic energy that is subsequently transferred to the surrounding gas via inelastic collisions. This energy transfer modulates the local temperature field and, like the electrostrictive density grating, produces an index grating. This index-of-refraction grating coherently reflects the probe beam at the phase-matching angle. The temporal behavior of this reflected signal beam is seen to have a gradual decay as a result of diffusion with an oscillation superimposed upon it. The modulation of the grating reflectivity, responsible for this oscillation, is caused by the pressure waves induced by the local heating or electrostriction. Because of the geometry of the grating, two counterpropagating sound waves are generated. The signal modulation is a manifestation of the alternate constructive and destructive interference of the two waves as they pass through each other. These infinitesimally strong pressure waves propagate at the speed of sound and are the physical basis of our measurement technique. In this work, we present the first observation of transient grating signals produced by particulates. The particulates absorb optical energy from the pump beams and transfer this energy to the surrounding gas through vaporization followed by inelastic collisions between the soot fragments and the surrounding gas molecules. This modulates the local temperature field and, hence, produces an index grating.

II. Theory

The theory behind laser-induced grating techniques, in general, has been discussed elsewhere.[5] Here, we simply summarize the points relevant to TGS gas-phase thermometry. If two laser beams with linear, parallel polarization are spatially and temporally overlapped, an intensity grating will be formed in the medium with a grating spacing, Λ, given by

$$\Lambda = \lambda/2 \sin(\theta/2) \tag{1}$$

The coupling of the light-intensity grating to the target medium produces a modulation in the local index of refraction. This modulation acts like a diffraction grating that will Bragg scatter a properly phase-matched probe beam. It can be shown (see the Appendix) that the grating spacing is determined entirely by conditions outside of the test environment. Therefore, it is not necessary to correct the value of Λ for changing conditions (pressure, temperature, composition) inside the test cell that alter the local index of refraction.

The study of light scattering by index perturbations in fluids is decades old and in many respects quite mature.[21] We begin by recalling a well-known result for the scattering efficiency, η, of Bragg scattering in fluids, regardless of the origin of the grating[22]

$$\eta = I_{\text{signal}}/I_{\text{probe}} = G(\theta, r_{\text{pr}}, r_p)\sin^2[\pi(L/\lambda_{\text{pr}})\Delta n] \quad (2)$$

The geometric factor, $G(\theta, r_{\text{pr}}, r_p)$, includes the spatial profile and spatial overlap of the incident beams.[23] G depends on the angular separation of the pump beams, θ, and the radius of the pump, r_p, and probe, r_{pr}, beams. [If the pump beams are not temporally overlapped, a second multiplicative factor must appear in Eq. (2).[24]] For relatively weak diffraction, the case of interest here

$$\eta \approx G(\theta, r_{\text{pr}}, r_p)[\pi(L/\lambda_{\text{pr}})\Delta n]^2 \quad (3)$$

Several physical mechanisms will produce an optically induced index modulation, Δn.[5] For the work presented here, only two are of importance: thermalization and electrostriction. Of these two, thermalization dominated most of the combustion environment measurements described here. Typically, during thermalization, a target molecular species optically absorbs energy through an electronic transition. This creates an excited-state population grating. In any particular environment, it is possible to create a laser-induced population grating, provided that the grating period of the original field intensity grating is greater than the mean free path of the molecules in the gas. Via inelastic collisions, the absorbed energy is transferred to the other nonabsorbing gas species present, locally heating the gas and thereby producing a thermal grating. This, in turn, modulates the local density and, hence, the local index of refraction. We have observed the formation of thermal gratings via soot particles acting as blackbody absorbers. Primarily through vaporization and subsequent inelastic collisions, the soot particles transfer the absorbed energy to the surrounding gas. In brief, electrostriction is a nonresonant optical process in which molecules are impulsively accelerated toward regions of high field intensity. This molecular movement modulates the local density and, hence, the local index.[13] We note that the transient grating signal frequency caused by thermalization is f_B, whereas it is $2f_B$ for electrostriction. The thermalization process under the conditions of interest here is more efficient at modulating the local index of refraction than is electrostriction. Hence, when thermalization does occur, it tends to dominate the TGS signal. For either process, the TGS signal grows roughly quadratically with total pressure.

When the intensity grating interacts with the local fluid to form the index grating, the fluid responds hydrodynamically to re-establish local equilibrium. To make the connection between the general light-scattering result of Eq. (2) and the hydrodynamic behavior of the test fluid, we expand the index perturbation in terms of two fluid variables, whose fluctuations are statistically independent,[25] namely, density and temperature

$$\Delta n = \left(\frac{\partial n}{\partial \rho}\right)_T \Delta\rho + \left(\frac{\partial n}{\partial T}\right)_\rho \Delta T \quad (4)$$

As pointed out by Paul et al.,[14] the second term in Eq. (4) is quite small compared with the first. Therefore, in this report, we concentrate solely on the first term. As discussed in detail elsewhere,[26,27] the index of refraction of a gas can be rigorously expanded in terms of density

$$(n - 1)\rho^{-1} = A_n + B_n\rho + \cdots \quad (5)$$

where A_n and B_n are constants determined by the local gas mixture. For the gases of interest here, e.g., N_2, H_2O, CO, CO_2, O_2, and C_xH_y, both constants are positive. Combining Eqs. (3–5), the diffraction efficiency of the gratings of interest to us can be written as

$$\eta \approx G(\theta, r_{\text{pr}}, r_p)(\pi L/\lambda_{\text{pr}})^2(A_n + 2B_n\rho)^2\Delta\rho^2 \quad (6)$$

For any fluid, a change in the local temperature will produce a change in the local density. Hence, a thermal grating leads to a density grating. For example, under isobaric fluid conditions (this approximation holds when the thermalization time scale is less than the transit time for an acoutic wave across one grating fringe)

$$\Delta\rho = -\rho(\Delta T/T) \quad (7)$$

The local temperature increase produced by thermalization can be approximated as

$$\Delta T = \phi(\alpha/\rho C_p)2I\tau_p \quad (8)$$

The dimensionless factor, ϕ, is somewhat analogous to the quantum yield factor encountered in laser-induced fluorescence (LIF) work. At high pressures and temperatures, ϕ becomes nearly unity.

When electrostriction generates the TGS signal, the density perturbation is governed by[13]

$$\Delta\rho = C_T\Gamma_e I(1/4nc) \quad (9)$$

Typically, both $\Delta T/T$ and $\Delta\rho/\rho$ are less than 10^{-3}, making the TGS technique truly nonintrusive.

TGS thermometry is achieved by collecting the TGS signal in a time-resolved fashion. Analysis of the oscillatory frequency of the signal provides a direct measure of the local sound speed, which can then be related to temperature through Eq. (14). Several techniques can be used to determine the oscillation frequency of a TGS signal, for example, direct theoretical fitting of the data, determination of the Brillouin peak frequency of the power spectrum of the data, determination of the zeroes of the derivatives of the data, etc. The most direct way is through fitting of the data in the time domain. This takes advantage of the fact that the theoretical understanding of the transient grating signal is quite mature. Theoretical development of the TGS signal in time is achieved by solving the appropriate hydrodynamic equations, including the effects of the incident lasers. The fluid-dynamic expressions for the conservation of mass, momentum, and energy are written in the linearized form as a function of $\Delta\rho$ and ΔT.[19] To these equations are added terms describing the electrostrictive force of the light fields on the fluid and the energy deposition arising from absorption of the incident light.[13] Solutions of these equations for $\Delta\rho$ and ΔT have been reported by various authors. Boyd[13] presents his solutions in the frequency domain, whereas Dean,[18] Desai et al.,[17] Paul et al.,[14] Cummings et al.,[15] and Hubschmid et al.[16] present their solutions in the time domain. From Eq. (6) we see that the TGS signal will be proportional to $\Delta\rho^2$. The complete expression for $\Delta\rho$, including all of the grating dissipative effects,[7–12] the influence of the temporal pulse shape[14,15] and spatial extent of the pump lasers,[15] the effects of collisional energy transfer,[14] and the effects of the relative magnitudes of the pulse duration, coherence length, and relative pump beam delays,[28] is lengthy. Fortunately, accurate TGS thermometry can be achieved using an approximate expression that we present here. The expression is similar to, but more inclusive than, the approximate expressions previously reported.[12,14,29] Including electrostrictive and thermal gratings, we find for the density perturbation, $\Delta\rho$

$$\Delta\rho(t) = A\exp(-D_t\mathbf{q}^2t) + B\exp[-(D_s\mathbf{q}^2 + Q + A_{\text{rad}})t] + C\exp(-\Gamma\mathbf{q}^2t - \beta^2t^2)\cos(\omega_B t) \quad (10)$$

It is customary to assign $t = 0$ to the arrival of the pump laser beams. In this case, $\Delta\rho(t \leq 0) = 0$. The first two terms in Eq. (10) describe a static thermal or entropy wave that dissipates via diffusion. The third term describes a propagating acoustic mode that dissipates via viscous damping.[30] The coefficients A, B, and C are simply used as fitting parameters when TGS thermometry is performed. The parameter β appearing in Eq. (10) is strictly for fitting convenience. It is used to correct for the fact that the laser beams have finite transverse spatial extent.

When pump lasers with nanosecond or longer pulse widths are employed, it is necessary to perform a convolution of the hydrodynamic response with the laser pulse shape. In practice, a suitable fit function, $f(t)$, for the TGS signal can be constructed as follows:

$$f(t) = \psi g_{\text{las}}(t) \circ \Delta\rho^2(t) \tag{11}$$

where $g_{\text{las}}(t)$ is usually taken to be a Gaussian. The open circle denotes a Laplace convolution over positive values of the time. Equation (11) assumes that the pump laser beams arrive in the target zone simultaneously. If one beam is delayed with respect to the other, then Eq. (11) must be modified.[24,28] In Fig. 1 we present an example of a fit to acquired TGS data using Eqs. (10) and (11).

When performing TGS thermometry by curve fitting the acquired signal, the first step is an accurate determination of the grating spacing. This can be done by direct measurement of the angular separation of the pump beams; however, we found it easier to acquire calibration signals under well-known gas conditions and then fit the signal using the grating spacing as a free parameter. An example of a calibration signal is shown in Fig. 1. Fitting of signals taken under test conditions is made in a two-step procedure. First, values for the thermodynamic quantities, D_t, D_s, and Γ, as well as the molecular parameters, Q and A_{rad}, are estimated. Then the experimental signal is fit using A, B, and C along with the frequency ω_B as fitting parameters. A final, best fit is then made by allowing the thermodynamic variables to change along with the scaling constants and the frequency.

Temperature can be extracted from a TGS measurement through the use of the ideal gas expression for the sound speed and the definition of the TGS frequency, respectively

$$C_s = \sqrt{RT(\gamma/M)} \tag{12}$$

$$f_B = m(C_s/\Lambda) \tag{13}$$

[Note that f_B is related to ω_B in Eq. (10) through $\omega_B = 2\pi f_B$.] In Eq. (13), $m = 1$ or 2 for thermal or electrostrictive signals, respectively. By inverting Eq. (12) and making use of the definition in Eq. (13), we can write an expression for the TGS experimentally determined temperature

$$T = f_B^2 \frac{\Lambda^2}{m^2}\left(\frac{M}{\gamma}\right)\frac{1}{R} \tag{14}$$

Using Eq. (14), we can estimate the uncertainty, σT, associated with TGS thermometric measurements. Formally, we find

$$\sigma T^2 = \left(\frac{\partial T}{\partial f_B}\right)^2 \sigma f_B^2 + \left(\frac{\partial T}{\partial \Lambda}\right)^2 \sigma\Lambda^2 + \left[\frac{\partial T}{\partial (M/\gamma)}\right]^2 \sigma\left(\frac{M}{\gamma}\right)^2 \tag{15}$$

where the derivatives are easily evaluated using Eq. (14). As a numerical example, consider $\sigma f_B = 3\%$ of f_B, $\sigma\Lambda = 1\%$ of Λ, and $\sigma(M/\gamma) = 5\%$ of M/γ. Then for $f_B = 60$ MHz, $\Lambda = 15$ μm, $M/\gamma = 20.53$, and $T = 2000$ K, $\sigma T = 161$ K or 8.1% of T. As noted next, the accuracy of the measured frequency can be improved. Using $\sigma f_B = 1\%$ of f_B in the preceding example gives $\sigma T = 115$ K or 5.7% of T.

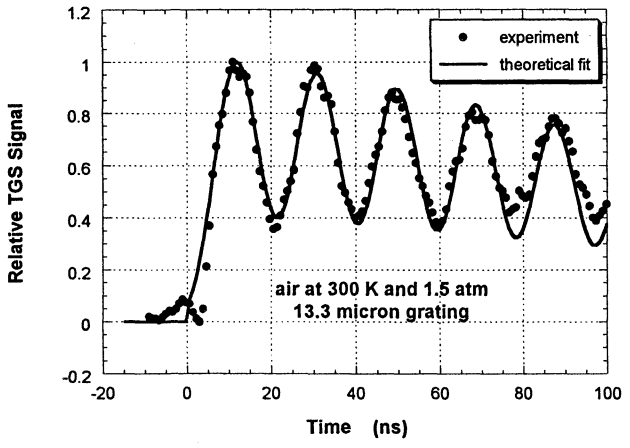

Fig. 1 Nonresonant TGS signal in air caused by electrostriction.

III. Experiments

To provide a stable, repeatable, high-pressure combustion environment in which to demonstrate the TGS technique, the high-pressure burner (HPB) was constructed. This flowing pressure vessel consists of a square steel tube, 12.7 cm on a side, 35 cm long, with 0.9 cm wall thickness encased in a water jacket. The internal pressure is regulated with a needle valve on the exhaust port of the vessel, and the HPB was operated over a pressure range from 1 to 9 atm. The flame was generated in a sintered bronze porous plug burner, 6.4 cm in diameter, also water cooled. The plug has a nitrogen coflow, but this was not used in most of the experiments, as the measurement location was centered over the burner and was less than 2 cm above the surface. To provide optical access, three BK-7 windows were mounted at 90 deg to each other in the horizontal plane, with the plug surface in the lower field of view. The two windows through which the laser beams pass were mounted on extension tubes.

Fuel and air were metered with high-pressure rotometers and mixed before entering the HPB. The reactant velocity at the surface of the plug was less than 1 m/s, and was laminar in all cases. In most test runs, only ethylene and air were used, and the equivalence ratio was varied between one (stoichiometry) and two. Because the signal strength scales nonlinearly with density, it was desirable to depress the flame temperature through dilution with nitrogen at the lower pressures. As the pressure increased, the reaction zone became thinner and the temperature gradient steeper at the burner surface. This increased the heat flux to the plug, resulting in cooler product gas temperatures at the measurement volume. In all cases, the temperatures measured with the thermocouple were very stable, with fluctuations less than 1% of the mean.

A breadboard TGS optical train was set up and coupled to the HPB as shown schematically in Fig. 2. The frequency doubled output of an Nd:YAG laser was split into two pump beams of equal energy (~7 ns pulse width) and passed through a 350-mm focusing lens. To ensure optimal grating formation, the optical paths of the two pump beams were matched to within a few millimeters. The 488-nm probe beam was directed toward the same lens parallel to the pump beams. During alignment of the detector, 4% of the probe beam was split off and directed at the lens to trace out the path of the actual TGS signal beam. At their crossover point, the pump beams formed an optical grating with a period of 10–14 μm. The pump and probe beams lay along the centerline of the burner and their height above the surface was varied from 6–16 mm. Two mirrors directed the signal beam through a spatial filter and two 488-nm laser line filters onto a photomultiplier tube. The pump, probe, and signal beams passed through uncoated

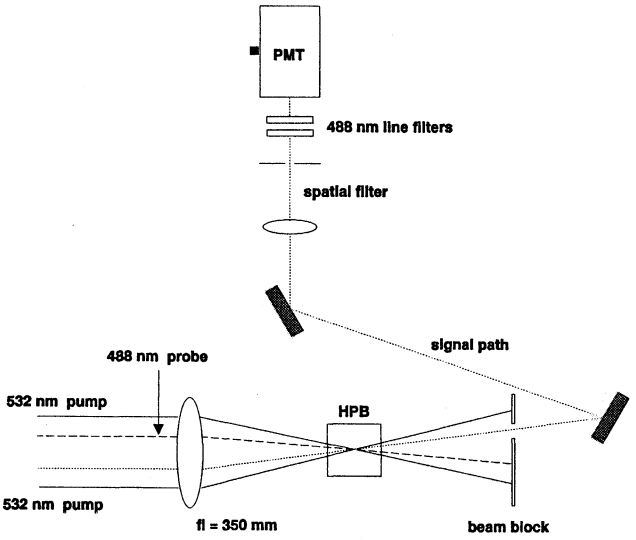

Fig. 2 Schematic of the TGS optical setup employed.

BK-7 windows that were 0.375 in. thick. The windows created stray light through diffuse scatter and specular reflection. The line filters rejected the unwanted 532-nm light at the detector and the spatial filter rejected the unwanted 488-nm light at the detector.

Initial alignment of the pump, probe, and signal tracer beams was achieved with the aid of a 100-μm pinhole placed at the crossover point of the beams. All four input beams were held parallel to each other before passing through the focusing lens. To facilitate separation of the actual signal beam from the pump and probe beams on the output side of the HPB, the probe and signal tracer beams were vertically displaced from the pump beams by about 1 cm on the front face of the focusing lens. The horizontal displacement between the two pump beams as they passed through the focusing lens was made as small as practically possible ($\sim$15 mm) with the equipment employed. The horizontal displacement between the probe and false signal beams was then fixed to ensure that they generated a grating spacing identical with that of the pump beams [refer to Eq. (1)], i.e., phase-matching conditions were met. Small adjustments were then made to the beam-directing mirrors to ensure that the beams maintained their proper horizontal spacing and simultaneously passed through the pinhole (phase matching). With this beam arrangement, the probe volume was defined as a long thin ellipsoid about 100 μm in diameter (at the widest point) and roughly 5 mm long.

Once the initial alignment was established, the HPB was filled at ambient temperature with either pressurized air or CO_2. The electrostrictive response from this static gas sample was used to optimize the TGS signal, and, through signal analysis, was used to accurately determine the actual grating spacing. We note that the choice of angular separation between the pump beams is a practical one based on two issues. First, the angular separation must be small enough to ensure that the fringe-to-fringe transit time of the sound waves is greater than the pulse width of the pump laser, otherwise the Doppler modulation of the signal is washed out. And, secondly, the angular separation must be great enough to ensure effective spatial separation of the signal from the incident beams.

After signal optimization, the burner was lit directly with a starter flame and stabilized near stoichiometric conditions at 1 atm. For this work, ethylene/air flames were used exclusively because of their propensity to soot as well as the high saturation pressure of ethylene. Flow rates for both gases were monitored with rotameters corrected for operation with these gases at elevated pressure. Once the flame was stabilized, an iterative process was used to reach high-pressure, sooting-flame conditions: the exhaust valve was partially closed on the HPB and the gas flow rates were increased. This procedure was repeated until desired pressure and sooting conditions were achieved. At this point, TGS signals were acquired with the use of a digital oscilloscope and saved into memory for later analysis with commercially available personal computer software programs. The signals shown herein were recorded by averaging over 24–64 laser shots. TGS measurements were made in burnt gases of sooting flames using 50 mJ of energy split between the two pump beams (532 nm) and 500 mW of power in the continuous wave (cw) probe beam (488 nm).

During this work, the transmitted cw probe beam was chopped and monitored with a photodiode to determine its extinction as a result of soot particles. With these extinction measurements we were able to estimate the upper limit of the soot volume fraction (SVF) present. Under slightly rich conditions (equivalence ratio $\sim$1.2), we found a SVF of $\sim$1 ppm; however, with increasing fuel to air ratios, the extinction measurements became compromised because of the design of the HPB. The window arms provided recirculation zones that quickly deposited soot on the windows as well as affected the length over which beam extinction was occurring. Therefore, we report no measured SVF values for the richest flames examined.

After verifying that TGS measurements could be made in a sooty environment, we sought to verify TGS thermometry in sooting flames. To this end, a B-type thermocouple (Pt/Rh) was inserted through the back wall of the HPB into the flame zone. The intersection of the three incident laser beams and the thermocouple bead were maintained at the same height above the burner surface. In the horizontal plane, the thermocouple bead was placed a couple of millimeters away from the beam intersection. Stable flames supported by this burner have been shown previously to be quite one dimensional (this conclusion is based on OH planar laser-induced fluorescence measurements taken at 1 atm in this burner), and so the horizontal distance between the beams and thermocouple bead is not a critical parameter.

For each of the stable flames studied, the thermocouple readings were observed to be very stable with changes on the order of $\leq$5°C over a period of a few minutes. The recorded thermocouple readings were later corrected to account for the energy balance between the thermocouple and the hot flame gases. Heat conducted from the gases to the thermocouple was balanced with radiation from the thermocouple back to the gases. These corrections were made with an estimated Nusselt number and an assumed spherical bead 1.3 mm in diameter with an emissivity of 0.15. For the flames employed, the radiation correction added an additional 13–16% to the observed thermocouple temperature reading.

IV. Discussion

The first goal of this work was the verification that TGS signals could be acquired in a soot-laden, high-temperature and pressure environment. Toward this end, TGS signals were acquired in the postreaction zone region of a heavily sooting ethylene/air premixed flame. TGS measurements were made at various pressures, stoichiometries, and axial locations in the burner. Typical TGS signals are shown in Fig. 3 for two heights above the burner surface, 6 and 16 mm, that exhibited very different local temperatures. The pressure and stoichiometry are different between these two flames, resulting in the difference in temperature. The normalized TGS signals acquired at these two axial locations are shown with the vertical axis displaced for clarity. Again, all of the temperature (and major species) information is contained in the oscillation frequency (and rate of decay), so that no information is lost by normalizing the signal amplitudes. The upper curve was obtained at 3.7 atm with an equivalence ratio of 1.7, whereas the lower curve was acquired at 7.6 atm with an equivalence ratio of about 1.3. For both signals, the soot volume fraction was greater than 1 ppm. Each of the signals was fitted with the

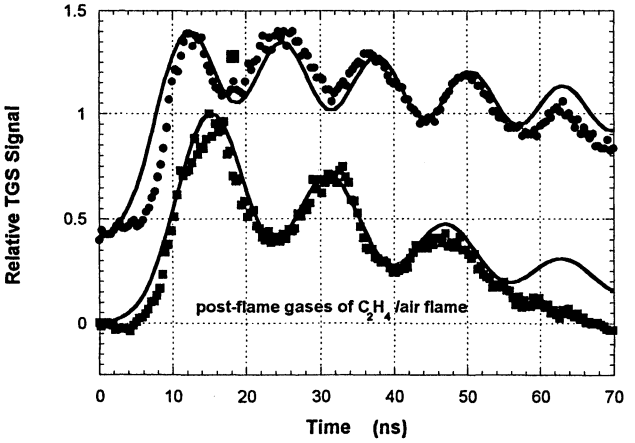

Fig. 3 Two examples of TGS signals acquired in sooting ethylene/air flames. The curves are displaced for convenience. Fits to the data are shown; they indicate temperatures of 1500 K (upper) and 960 K (lower).

complete TGS theory to extract the indicated temperature. In each case, the effective thermalization rate required for a good fit was a good order of magnitude lower than the corresponding elastic gas kinetic collision rate. This suggests (not surprisingly) that the transfer of energy from the soot particles to the surrounding gas occurs in a multistep fashion. Additionally, for soot concentration values larger than 1 ppm, the modulation depth of the oscillations is reduced relative to that for lower concentration values. This is another indication of a more complex energy transfer process than the single-step process assumed by the model.[14]

Referring back to Eq. (14), when performing TGS thermometry, the frequency, f_B, is the experimentally measured quantity, Λ is a parameter set by design, and R is a constant. The ratio of M to γ is not measured and must be estimated. For a particular fuel and oxidizer this is not difficult and can be done using simple chemistry considerations. Both M and γ are simple sums of the corresponding values for the major gas mixture components weighted by the relative mole fractions, and γ exhibits an explicit temperature dependence as well. For hydrocarbon/air flames, the ratio does not vary greatly with either equivalence ratio or temperature. For example, in Table 1, we show the calculated values for M/γ for ethylene/air flames over the ranges of equivalence ratios between 1 and 2 and temperatures between 1000 and 2000 K. The percentage difference of these M/γ values with respect to the value at equivalence ratio 1.5 and $T = 1500$ K are shown in parentheses for each table entry. As seen, these values differ by 10% or less over the full range. Similar results can be found for other hydrocarbon/air flames. They reflect the fact that for any of these flames, the major exhaust gas constituents will be N_2, H_2O, CO, and CO_2.

Empirical expressions for the individual values of γ_i for each combustion gas are easily determined from tabulations found in the literature.[31] To estimate the mole fractions of the major species in our flame environments, we used the output of the CET89 combustion equilibrium code.[32] For equivalence ratios greater than one, the major species in the flame zone are found to be N_2, CO, and H_2O. Nitrogen accounts for at least 58% of the total number density for equivalence ratios greater than one.

Strictly speaking, Eq. (12) expresses the sound speed for ideal gases, and its accuracy should be examined for pressures of interest to the combustion community. As shown in the Appendix, Eq. (12) is a very good approximation for C_2H_4/air flames. For a temperature of 1500 K, the deviation of the sound speed from the ideal gas value is less than 3% for pressures up to 70 atm. Similar results can be expected for other hydrocarbon/air flames.

In Fig. 4, we show the TGS signal acquired in an ethylene/air flame at 7.9 atm at an equivalence ratio of 1.6. The signal was acquired 10 mm above the burner surface in the burnt gas region using a 30-laser-shot average (3 s). The signal shows no detectable indication of electrostriction and, therefore, is a result of a thermal grating arising from blackbody absorption by the soot. This observation is not surprising. The thermalization process is more efficient than the electrostriction process at producing the local index modulation. Three oscillations are clearly discernible in the signal that was acquired simultaneously with a thermocouple reading taken at the same height. With the computed mole fractions of the flame code and the literature values for γ_i, we easily calculated a value of M/γ (23.3 ± 1.2 g/mol), including the N_2 diluent for the gas mixture, and extracted a temperature, using Eq. (14), with a measured grating spacing of 13.3 μm. The inferred TGS temperature of 1740 ± 140 K agrees with the corrected thermocouple temperature of 1710 ± 75 K. The uncertainty in the TGS temperature here is largely determined by the uncertainty in the oscillation frequency of 3%. The oscillation frequency was found using three methods: 1) direct fitting of the theory to the measurement, 2) analysis of the autocorrelation function, and 3) use of a peak finder algorithm. The 3% uncertainty reported reflects the spread in these three frequency determinations. This uncertainty reflects the relatively low amplitude modulation of the signal. Note that the experimental modulation depth is less than that predicted by the model fit. This was not the case in the calibration files taken with no soot present (refer to Fig. 1). This discrepancy may be caused by the thermalization process that soot undergoes during thermal grating generation. At the pump laser intensities employed here, the individual soot particles vaporize after absorbing the pump la-

Table 1 Calculated values for M/γ for ethylene/air flames[a]

Equivalence ratio	T, K				
	1000	1250	1500	1750	2000
1.00	21.79	22.08	22.27	22.37	22.47
	(−6.9)	(−8.1)	(−8.9)	(−9.3)	(−9.7)
1.25	20.88	21.14	21.32	21.46	21.55
	(−2.8)	(−4.1)	(−4.9)	(−5.5)	(−5.9)
1.50	19.84	20.12	20.28	20.41	20.53
	(2.2)	(0.8)	(0.0)	(−0.6)	(−1.2)
1.75	18.98	19.23	19.38	19.49	19.65
	(6.9)	(5.5)	(4.7)	(4.1)	(3.3)
2.00	18.18	18.42	18.59	18.69	18.87
	(11.6)	(10.1)	(9.1)	(8.5)	(7.5)

[a]Using CET89, that includes all relevant equilibrium chemistry and transport.[32] Note, these calculations were made assuming no added N_2 diluent.

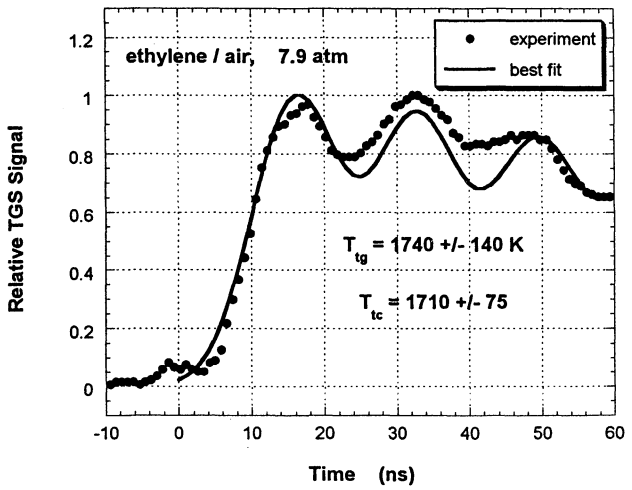

Fig. 4 Transient grating signal acquired in the burnt gases of a rich (ϕ = 1.6) flame. The T_{tg} agrees with T_{tc}.

ser light.[33-35] The soot vapor consists primarily of C_2 and C_3 molecules (some larger graphitic fragments may be present as well) that perturbatively heat the surrounding gas through inelastic collisions. Therefore, thermal grating formation via soot is a multistep process. Previous work by Paul et al.[14] suggests that multistep thermalization decreases the amplitude of the acoustic waves relative to the thermal (entropy) wave. The net effect is a reduction in the signal modulation depth as seen here. In practice, this modulation depth can be increased by increasing the grating spacing. It should be noted that the C_2 and C_3 soot fragments do not have absorption features that are resonant with 532-nm pump beams.

For the measurement shown in Fig. 4, we estimated $\Delta T/T$ to be 2×10^{-5}. This value was found using Eqs. (6) and (7) with the following parameter values: $G = 0.125$ (following Siegman[23]), $L = 5$ mm, $\lambda_{pr} = 514.5$ nm, $A_n = 6.69$ cm^3/mol, and $B_n = 8.959$ cm^6/mol (after Refs. 25 and 26), and $\rho = 5.5 \times 10^{-5}$ mol/cm^3. The scattering efficiency was determined directly from the raw data to be $\eta = 6.5 \times 10^{-9}$. Hence, for this measurement, the technique is clearly nonintrusive.

For equivalence ratios of 1.9 and 2.0, the richest conditions examined here, we found that the inferred TGS temperature was significantly and consistently lower than the thermocouple temperature. At 1.9, the transient grating temperatures were low by 19%, and at 2.0 they were low by 25%. This observation suggests that at very high soot loadings, the TGS technique may cease to be nonintrusive. If significant amounts of C_2 and C_3 are vaporized into the bright fringe planes, the local density will certainly be modified; however, this will only alter the amplitude of the signal by increasing it without affecting the frequency. The frequency will be altered if there are sufficient soot fragments present to modify the local value of M/γ. To check the reasonableness of this idea, we performed the coarse calculation outlined in the Appendix to estimate the SVF needed to raise the extracted temperature to the level indicated by the thermocouple readings.

It is well known that for modest fluences, the light absorbed from a laser beam by soot particles rapidly heats the particles to their vaporization temperature.[33] The expelled vapor, consisting largely of C_2 and C_3, displaces the local combustion gases over a volume with a radius on the order of one mean-free path.[34] Under our pressurized flame conditions, the mean-free path is approximately 0.05 μm or 1/260th of the width of a single grating fringe. The collision rate is quite high (about 23 GHz), and so the C_n ($n = 2$ or 3) molecules are very rapidly mixed with combustion gases over a short distance. An estimated diffusion coefficient[36] of 0.3 cm^2/s for C_n in N_2 indicates that over the pulse width of the pump laser (10 ns), the C_n molecules will be displaced by 1.3 μm, or roughly one-tenth of the width of a single grating fringe caused by random walk movements. For flame-zone thermometry, the total time period required of a TGS signal is less than 100 ns (refer to Fig. 4). During this time, the C_n molecules would diffuse a distance less than or equal to the fringe spacing. Hence, most of the expelled C_n will remain inside the fringe containing the parent soot molecule during a TGS measurement. The pump laser operated at 10 Hz in our measurements. During the time between pulses, the molecules in a given fringe are convectively swept out of the target volume; therefore, it is not necessary to account for C_n accumulation over several laser shots.

We sought to estimate the amount of material in the soot vapor produced by the pump laser beams and its contribution to the overall value of M/γ. (The intensity in the probe laser beam is seven orders of magnitude less than that in the pump laser beams, and so we ignore it here.) The dynamics of laser/soot interactions have been studied previously.[33-35] Both the complete and approximate theoretical results agree well with the experiment.[34,35,37,38] To simplify the required calculations, we made use of Eckbreth's approximate dynamic solution[35] for the radius of a soot particle as a function of time during laser irradiation. The radius at time t is calculated from the initial radius and an exponential factor that arises when one equates the optical energy absorbed by a soot particle to the energy lost via vaporization, a very reasonable assumption.[33,34] That is, energy loss via conduction is much less (~10% of the total loss) than that lost by vaporization and is safely ignored.[35] This model provides a means to estimate the volumetric loss of a soot particle in the presence of our pump lasers. Because the mass density of a soot particle is well known, the model in turn tells us the amount of C_n expelled as vapor during a pump laser pulse.

Using tabulated values[39] of γ for C_n and expressions (A5–A8), we calculated a value of M/γ for the combined combustion–gas/C_n mixture. We note that for our experimental conditions, $a(\tau_{las}) \ll a_0$. This results in our calculational findings being insensitive to a_0 when Eqs. (A6) and (A7) are substituted into Eq. (A5). Our numerical procedure was then reduced to calculating M/γ as a function of the soot volume fraction, f_v. All other parameters were fixed by the experimental conditions. For each flame condition considered, we varied f_v until the extracted TGS temperature agreed with the thermocouple temperature. (This corresponded to an increase in the value of M/γ on the order of 15%.) For example, in an 8.8-atm flame with an equivalence ratio of 1.9, we measured a thermocouple temperature of 1735 $\pm$ 75 K and a TGS temperature of 1620 $\pm$ 160 K. Using the experimental pump energy as input and assuming a soot vapor of pure C_3, we estimate that a SVF of 23 ppm will produce a temperature of 1735 K. For a pure C_2 vapor, we estimate that an SVF of 45 ppm will yield $T = 1710$ K. Similarly, for a 50/50 mix of C_2 and C_3, $f_v = 30$ ppm produces $T = 1735$ K. Laser-beam extinction measurements by other workers (see Fig. 2 in Ref. 38) have found SVF values of 10 ppm for rich ethylene/air flames at 1 atm. Because f_v is expected to increase with pressure, we find these computational results to be quite reasonable.

Generalization of the preceding numerical considerations requires a careful assessment of the affect of three key parameters, namely, the incident laser intensity, the gas density, and the soot volume fraction. We do not attempt such a comprehensive calculation here. We can, however, anticipate that the influence of the soot vapor on the local temperature will decrease with increasing gas density or with decreasing laser intensity or decreasing SVF. We fully expect that TGS will be a viable nonintrusive diagnostic at high pressure.

V. Conclusions

We have successfully demonstrated that the local gas-phase temperature can be extracted from nonresonant TGS measurements made in high-pressure, sooting, premixed combustion environments. Soot particles, acting as blackbody absorbers, contribute to a thermal grating signal. For an ethylene/air flame with an equivalence ratio of 1.6, we found good agreement between the extracted TGS temperature and simultaneously corrected thermocouple measurements. For equivalence ratios between 1.9 and 2.0, we found that the extracted temperatures were consistently lower than the thermocouple temperatures. We believe this discrepancy is because the soot particles influence the inferred temperature of the thermal grating signal if their relative concentration is sufficiently high. This contribution arises from a change in the local value of M/γ as a result of the expelled carbon fragments, C_2 and C_3, formed during the laser-induced vaporization of the soot particles.

Appendix: Analysis Details

The index of refraction inside the HPB will change with changing conditions of density and gas composition. It is necessary therefore, to consider whether or not the laser-induced grating spacing changes with a changing test environment. Because both pump beams pass symmetrically through the system (laboratory to window to burner assembly interior) it is suffi-

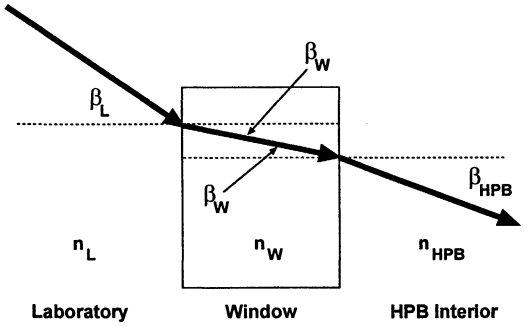

Fig. A1 Schematic of one pump beam path as it passes from the laboratory through the burner window into the HPB itself. The angles and indices of refraction needed for Snell's law are denoted by β_i and n_i, respectively.

cient to discuss only the path of one, as indicated in Fig. A1. Using Eq. (1) we can write the grating spacing inside the HPB as

$$\Lambda = \lambda_{\mathrm{HPB}}/2\,\sin(\beta_{\mathrm{HPB}}) \tag{A1}$$

(Note that we are now using the half angle rather than full angle between the beams.) Using the fact that $\lambda_{\mathrm{HPB}} = \lambda_L/n_{\mathrm{HPB}}$ and that (Snell's law)

$$n_L \sin(\beta_L) = n_W \sin(\beta_W) = n_{\mathrm{HPB}} \sin(\beta_{\mathrm{HPB}}) \tag{A2}$$

we can rewrite Eq. (A1) as follows:

$$\Lambda = \frac{\lambda_L}{2n_{\mathrm{HPB}} \sin(\beta_{\mathrm{HPB}})} = \frac{\lambda_L}{2n_L \sin(\beta_L)} \tag{A3}$$

As seen in Eq. (A3), the grating spacing is determined entirely by the conditions outside of the test region. Hence, the grating spacing is a laboratory-controlled constant.

Extraction of the local temperature from a transient grating experiment makes use of the ideal gas expression for the speed of sound. To examine the suitability of the ideal gas expression for gases at elevated pressure, we employed a virial expansion of Eq. (12) written as[40]

$$C_s^2 = \frac{\gamma_0 RT}{M}\left\{1 + \frac{1}{V_m}\left[2B + 2(\gamma_0 - 1)T\frac{\partial B}{\partial T} + \frac{(\gamma_0 - 1)^2}{\gamma_0} T^2 \frac{\partial^2 B}{\partial T}\right] + \cdots\right\} \tag{A4}$$

where γ_0 denotes the ideal gas value of the specific heat ratio. The right-hand side of Eq. (A4) was evaluated using virial data[41] along with extrapolation and mixture estimation methods[36] found in the literature. For example, for $T = 1500$ K and mole fractions of 0.60, 0.17, 0.13, and 0.10 for N_2, CO, H_2O, and CO_2, respectively, we calculate that $\gamma = 1.285$ and $B = 24.6$ cm^3/mol. Equation (A4) then indicates a deviation in the sound speed from the ideal gas value of 1% at 24.5 atm and 5% at 124.5 atm. Hence, the ideal gas approximation for the sound speed is a good one for our test environment and most practical combustors.

Estimating the density and mole fraction of carbon fragments, C_n, in the target volume following laser-induced soot vaporization, can be made as follows. The C_n number density, N_{C_n}, can be written as

$$N_{C_n} = N_A M_{\mathrm{vap}} N_{\mathrm{part}} \tag{A5}$$

Using Eckbreth's dynamic model,[35] we calculate M_{vap} from the following:

$$M_{\mathrm{vap}} = \frac{\frac{4}{3}\pi[a_0^3 - a(\tau_{\mathrm{las}})^3]\rho_{\mathrm{part}}}{m_{C_n}} \tag{A6}$$

The soot particle number density, N_{part}, can be cast as a function of the initial particle radius and f_v

$$N_{\mathrm{part}} = (6/\pi)(f_v/a_0^3) \tag{A7}$$

Finally, the C_n mole fraction, x_{C_n}, is found from

$$x_{C_n} = \frac{N_{C_n}}{N_{C_n} + N_{\mathrm{gases}}} \tag{A8}$$

Acknowledgment

Support for this program was provided under U.S. Air Force Contract F33615-97-C-2707.

References

[1]Cummings, E. B., Hornung, H. G., Brown, M. S., and DeBarber, P. A., "Measurement of Gas-Phase Sound Speed and Thermal Diffusivity over a Broad Pressure Range Using Laser-Induced Thermal Acoustics," *Optics Letters*, Vol. 20, No. 14, 1995, pp. 1577, 1578.

[2]Eckbreth, A. C., *Laser Diagnostics for Combustion Temperature and Species*, Section 6.7, Gordon and Breach, Amsterdam, 1996.

[3]Hall, R. J., and Boedecker, L. R., "CARS Thermometry in Fuel-Rich Combustion Zones," *Applied Optics*, Vol. 23, No. 9, 1984, pp. 1340–1346.

[4]Martinsson, L., Bengtsson, P.-E., Alden, M., and Kroll, S., "Applications for Rotational CARS for Temperature Measurements at High Pressure and in Particle-Laden Flames," *Temperature, Its Measurement and Control in Science and Industry*, edited by J. F. Schooley, Vol. 6, American Inst. of Physics, New York, 1992.

[5]Eichler, H. J., Gunter, P., and Pohl, D. W., *Laser-Induced Dynamic Gratings*, Springer–Verlag, Berlin, 1986.

[6]Zhu, X. R., McGraw, D. J., and Harris, J. M. "Holographic Spectroscopy, Diffraction from Laser-Induced Gratings," *Analytical Chemistry*, Vol. 64, No. 14, 1992, pp. 710A–719A.

[7]Salcedo, J. R., Siegman, A. E., Dlott, D. D., and Fayer, M. D., "Dynamics of Energy Transport in Molecular Crystals: The Picosecond Transient-Grating Method," *Physical Review Letters*, Vol. 41, No. 2, 1978, pp. 131–134.

[8]Tanaka, H., Sonehara, T., and Takagi, S., "A New Phase-Coherent Light Scattering Method: First Observation of Complex Brillouin Spectra," *Physical Review Letters*, Vol. 79, No. 5, 1997, pp. 881–884.

[9]Yan, Y. X., Cheng, L. T., and Nelson, K. A., "The Temperature-Dependent Distribution of Relaxation Times in Glycerol: Time-Domain Light Scattering Study of Acoustic and Mountain-Mode Behavior in the 20-MHz-3 GHz Frequency Range," *Journal of Chemical Physics*, Vol. 88, No. 10, 1988, pp. 6477–6486.

[10]Brown, M. S., DeBarber, P. A., Cummings, E. B., and Hornung, H. G., "Trace Species Concentration and Temperature Measurements at High Pressure Using Laser-Induced Grating Spectroscopy," Society of Photo-Optical Instrumentation Engineers, Paper 2546-72, San Diego, CA, July 1995.

[11]Dreizler, A., Dreier, T., and Wolfrum, J., "Thermal Grating Effects in Infrared Degenerate Four-Wave Mixing for Trace Gas Detection," *Chemical Physics Letters*, Vol. 233, No. 5–6, 1995, pp. 525–532.

[12]Williams, S., Rahn, L. A., Paul, P. H., Forsman, J. W., and Zare, R. N., "Laser-Induced Thermal Grating Effects in Flames," *Optics Letters*, Vol. 19, No. 21, 1994, pp. 1681–1683.

[13]Boyd, R. W., *Nonlinear Optics*, 1st ed., Academic, Boston, MA, 1992, Chap. 8.

[14]Paul, P. H., Farrow, R. L., and Danehy, P. M., "Gas-Phase Thermal-Grating Contributions to Four-Wave Mixing," *Journal of the Optical Society of America, B*, Vol. 12, No. 3, 1995, pp. 384–392.

[15]Cummings, E. B., Leyva, I. A., and Hornung, H. G., "Laser-Induced Thermal Acoustics (LITA) Signals from Finite Beams," *Applied Optics*, Vol. 34, No. 18, 1995, pp. 3290–3302.

[16]Hubschmidt, W., Hemmerling, B., and Stampanoni-Panariello, A., "Rayleigh and Brillouin Modes in Electrostrictive Gratings," *Journal of the Optical Society of America, B*, Vol. 12, No. 10, 1995, pp. 1850–1854.

[17]Desai, R. C., Levenson, M. D., and Barker, J. A., "Forced Ray-

leigh Scattering: Thermal and Acoustic Effects in Phase-Conjugate Wave-Front Generation," *Physical Review A: General Physics*, Vol. 27, No. 4, 1983, pp. 1968–1976.

[18]Dean, D. R., "Optically Induced Diffraction Gratings in Liquids and Solids," Technical Report Prepared for the Office of Naval Research, National Technical Information Service, AD-767-076, Springfield, VA, Aug. 1973.

[19]Mountain, R. D., "Spectral Distribution of Scattered Light in a Simple Fluid," *Review of Modern Physics*, Vol. 38, No. 1, 1966, pp. 205–214.

[20]Grubbs, W. T., and MacPhail, R. A., "High Resolution Stimulated Brillouin Gain Spectrometer," *Review of Scientific Instruments*, Vol. 65, No. 1, 1994, pp. 34–41.

[21]Berne, B. J., and Pecora, R., *Dynamic Light Scattering*, Krieger, Malabar, FL, 1990.

[22]Yariv, A., *Optical Electronics*, Saunders College Publishing, Philadelphia, PA, 1991, Chap. 12.

[23]Siegman, A. E., "Bragg Diffraction of a Gaussian Beam by a Crossed-Gaussian Volume Grating," *Journal of the Optical Society of America*, Vol. 67, No. 4, 1977, pp. 545–550.

[24]Trebino, R., Gustafson, E. K., and Siegman, A. E., "Fourth-Order Partial-Coherence Effects in the Formation of Integrated-Intensity Gratings with Pulsed Light Sources," *Journal of the Optical Society of America, B*, Vol. 3, No. 10, 1986, pp. 1295–1304.

[25]Berne, B. J., and Pecora, R., *Dynamic Light Scattering*, Krieger, Malabar, FL, 1990, Chap. 10.

[26]Buckingham, A. D., and Graham, C., "The Density Dependence of the Refractivity of Gases," *Proceedings of the Royal Society of London, Series A: Mathematical and Physical Sciences*, Vol. 336, 1974, pp. 275–291.

[27]Burns, R. C., Graham, C., and Weller, A. R. M., "Direct Measurement and Calculation of the Second Refractivity Virial Coefficients of Gases," *Molecular Physics*, Vol. 59, No. 1, 1986, pp. 41–64.

[28]Stampanoni-Panariello, A., Hemmerling, B., and Hubschmid, W., "Electrostrictive Generation of Nonresonant Gratings in the Gas Phase by Multimode Lasers," *Physical Review A: General Physics*, Vol. 51, No. 1, 1995, pp. 655–662.

[29]Cummings, E. B., "Laser-Induced Thermal Acoustics: Simple Accurate Gas Measurements," *Optics Letters*, Vol. 19, No. 17, 1994, pp. 1361–1363.

[30]Morse, P. M., and Ingard, K. U., *Theoretical Acoustics*, Princeton Univ. Press, Princeton, NJ, 1968, Chap. 13.

[31]Keenan, J. H., Chao, J., and Kaye, J., *Gas Tables, International Version*, Wiley, New York, 1983.

[32]Gordon, S., and McBride, "Computer Program for Calculation of Complex Chemical Equilibrium Compositions, Rocket Performance, Incident and Reflected Shocks, and Chapman-Jouget Detonations," NASA SP-273, Washington, DC, 1971.

[33]Melton, L., "Soot Diagnostics Based on Laser Heating," *Applied Optics*, Vol. 23, No. 13, 1984, pp. 2201–2208.

[34]Dasch, C. J., "Continuous-Wave Probe Laser Investigation of Laser Vaporization of Small Soot Particles in a Flame," *Applied Optics*, Vol. 23, No. 13, 1984, pp. 2209–2215.

[35]Eckbreth, A. C., "Effects of Laser-Modulated Particulate Incandescence on Raman Scattering Diagnostics," *Journal of Applied Physics*, Vol. 48, No. 11, 1977, pp. 4473–4479.

[36]Reid, R. C., Prausnitz, J. M., and Poling, B. E., *The Properties of Gases and Liquids*, 4th ed., McGraw–Hill, New York, 1987, Chap. 11.

[37]Pinson, J. A., Mitchell, D. L., Santoro, R. J., and Litzinger, T. A., "Quantitative, Planar Soot Measurements in a D.I. Diesel Engine Using Laser-Induced Incandescence and Light Scattering," Society of Automotive Engineers, Paper 932650, Warrendale, PA, 1993.

[38]Mewes, B., and Seitzman, J. M., "Soot Volume Fraction and Particle Size Measurements with Laser-Induced Incandescence," *Applied Optics*, Vol. 36, No. 3, 1997, pp. 709–717.

[39]Lide, D. R. (ed.), *CRC Handbook of Chemistry and Physics*, CRC Press, Boca Raton, FL, 1993, pp. 5–51.

[40]Hirschfelder, J. O., Curtiss, C. F., and Bird, R. B., *Molecular Theory of Gases and Liquids*, Wiley, New York, 1954, pp. 230–232.

[41]Dymond, J. H., and Smith, E. B., *The Virial Coefficients of Pure Gases and Mixtures*, Clarendon, Oxford, England, UK, 1980.